Journal of Colloid and Interface Science 437 (2015) 291–296

Contents lists available at ScienceDirect

Journal of Colloid and Interface Science

www.elsevier.com/locate/jcis

Two-dimensional colloidal crystal assisted formation of conductive porous gold films with flexible structural controllability

Zhicheng Lu, Chen Liu, Heyou Han *

State Key Laboratory of Agricultural Microbiology, College of Science, Huazhong Agricultural University, Wuhan 430070, PR China

ARTICLE INFO

Article history:
Received 30 April 2014
Accepted 17 September 2014
Available online 30 September 2014

Keywords:
Polystyrene colloid particle
Two-dimensional colloidal crystal
Polyelectrolyte
Layer by layer assembly
Au nanoparticle
Electroless deposition
Two-dimensional conductive porous Au film

ABSTRACT

Two-dimensional (2D) colloidal crystals of polystyrene (PS) particles were used as a structure-controlling template to fabricate conductive Au films with an ordered array of nanoholes. The fabrication mainly involved the functionalization of the supporting substrate with polyelectrolyte (PE) functional layers, self-assembly of Au nanoparticles, and electroless deposition of gold. The self-assembly of Au nanoparticles and electroless deposition of gold were macroscopically monitored using ultraviolet–visible (UV–vis) spectroscopy based on the changes in both the extinction spectra of Au nanoparticles and the optical responses of ordered arrays of PS particles. By scanning electron microscopy (SEM) characterization, it was found that Au nanoparticles were assembled into a film structure with orderly dispersed nanoholes and the deposition of gold was confined to the preformed Au nanoparticle films. During the formation of Au films, PE layer structure, Au nanoparticle size and heating treatment applied to the PS template could influence the structures of conductive porous Au films such as the hole diameter, film thickness, and hole diameter/wall thickness ratio (D/W). In addition, this paper also described electrochemical cyclic voltammetry (CV) employed to demonstrate the porosity of the ultimate Au films.

1. Introduction

Porous metal films, or 2D metal films with orderly arranged pores, possess many novel properties. Thick porous metal films support extraordinary optical transmission (EOT) [1], where the intensity of the transmitted incident electromagnetic wave is several orders higher than that predicted by the traditional diffractive theory. Therefore, the films can be used to construct label-free biosensors as refractive-sensitive materials [2,3] or enhance spectroscopic signals as a substrate [4–6]. Metal films with ordered spherical voids strongly concentrate electromagnetic fields and have been used as plasmonic materials [7,8]. Conductive metal electrodes with nanoscale holes can reduce nonspecific signals [9] or increase the detection sensitivity of electrochemical sensors [10]. Metallic nanomesh can also be used as stretchable and transparent electrodes [11–13] or as an etching template in metal-assisted chemical etching of silicon [14,15].

Up to now, various preparation methods have been developed to meet the constantly growing demand for structural control of porous metal films. Porous metal films can be prepared using electron beam lithography (EBL) [16] with accurately regulated structures. Physical etching of the polymer sphere template combined with the physical deposition technique is also effective to fabricate porous metal films with strong structural controllability [17]; however, physical techniques based on precision instruments are usually required. Electrodeposition of metal under the guidance of the colloidal particle arrays is a parallel process [18] in which metal ions are reduced by electrons at the electrode surface and crystallized on the electrode surface; the structural adjustment capability of the final porous metal films, however, has been restricted by the metallic electrochemical growth characteristics, by which metal grows thick closely around the template and forms absolute spherical voids. Another type of method for preparing of porous metal films does not need precision equipment, such as the breath figures [19–23] and electroless deposition [24]. The breath figure method is only effective for the assembly of hydrophobic nanoparticles into honeycomb-like films. The electroless deposition process is constrained by tedious structural-controlling ability because metal growth is the same as in the electrodeposition process. Therefore, exploring novel methods to prepare porous metallic films with a better structure-controlling ability is highly desirable to deeply exploit the potential of 2D metal films.

Two-dimensional colloidal crystals of only single-sphere thickness have been a widely used as a framework to prepare various nanoscale replicas or reverse structures [25]. Using 2D colloidal

* Corresponding author. Fax: +86 27 87288505.
E-mail address: hyhan@mail.hzau.edu.cn (H. Han).

http://dx.doi.org/10.1016/j.jcis.2014.09.058
0021-9797/

crystals as a template to direct re-condensation of raw materials to obtain objective structures is a parallel process compared with time-consuming techniques such as EBL [26]. The 2D array of colloidal particles can be used in quasi-triangular threefold holes formed by three particles [27], the contact area between array particles and the supporting substrate [28,29], transverse waist of the array [30], and the bottom interstice space [31]. Commonly, the 2D array is composed of polymer particles and the structure of available sites in the 2D array can be adjusted by a series of modification means, making the template-directed nanofabrication method very flexible. For example, etching a 2D polystyrene (PS) array can convert a usable site from a threefold hole to a waist gap [32]; heating treatment, in contrast, can tune the shape of a threefold hole from the quasi-triangle shape to a circular shape [33].

In this paper, 2D colloidal crystals of PS particles were combined with PE functional layers, self-assembly of Au nanoparticles, and metal electroless deposition to fabricate 2D conductive porous Au films with the aim of achieving easy fabrication and flexible control over the structures of the final Au films. The assembly of Au nanoparticles and electroless deposition of Au was characterized by UV–vis spectroscopy and SEM. To demonstrate the structural modulation capacity of the template-directed nanoparticle-catalyzed electroless deposition method over the structure of porous Au films, the influential factors were investigated by SEM, atomic force microscopy (AFM) and transmission electron microscopy (TEM). The influence factors include the PE layer feature, Au nanoparticle size, and heating treatment to the PS array. Electrochemistry was further used to evaluate the porosity of conductive porous Au films.

2. Experimental section

2.1. Materials

Poly(diallyldimethylammonium chloride) (PDDA, Mw = 200,000–350,000) and poly(sodium 4-styrenesulfonate) (PSS, M.w. ~ 70,000) were purchased from Sigma Aldrich; poly(-acrylic acid) (PAA, M.W. ~ 240,000) were purchased from Alfa Aesar; styrene, potassium persulfate ($K_2S_2O_8$), sodium dodecyl sulfonate (SDS), sodium hydroxide (NaOH), absolute ethanol (C_2H_6O), chloroauric acid tetrahydrate ($HAuCl_3{\cdot}4H_2O$), trisodium citrate dihydrate ($C_6H_5Na_3O_7{\cdot}2H_2O$), sodium borohydride ($NaBH_4$), hydroxylamine hydrochloride ($NH_2OH{\cdot}HCl$), and concentrated sulfuric acid (H_2SO_4, 98 wt%) were of reagent grade and purchased from Sinopharm Chemical Reagent Co.; all aqueous solutions were prepared with ultra-pure water (resistance: 18.2 MΩ cm).

2.2. Apparatus

SEM characterization was performed on an FEI Inspect S electron microscope at an accelerating voltage of 30 kV. UV–vis spectra were obtained on a TU-1901 UV–vis spectrometer (Purkinje General Instrument Co., Ltd., China). Surface morphology was characterized in tapping mode with a Dimension 3100 AFM. TEM was performed on a Hitachi H-7650 transmission electron microscope at an acceleration voltage of 60 kV. Electrochemical experiments were carried out on a Princeton VersaStatTM 3 Potentiostat.

2.3. Preparation of conductive porous Au films

Glass slides were first treated in a piranha solution (V30% H_2O_2: V98% H_2SO_4 = 3:7) at 100 °C for 30 min and then thoroughly washed with and stored in ultrapure water before use. The preparation process of conductive porous films was shown in Scheme 1. For adsorption of polyelectrolyte layers, the substrates were alternately immersed in solutions of positively charged PDDA and negatively charged polyelectrolyte (PSS or PAA) for 15 min and then rinsed with ultrapure water for 5 min after each adsorption operation (Step I). All PE solutions had a concentration of 1 mg/mL (with respect to the repeated unit) and contained 0.5 M NaCl. The PDDA and PSS solutions were at pH 7 and the pH value of the PAA solution was adjusted to 2.5 using concentrated HCl. 2D arrays of PS particles were prepared by the interface assembly method [34] and transferred onto the PE layer modified substrates (Step II). The heating treatment of the PS array was performed on a hotplate at 120 °C. The substrates with PE layers/PS array were immersed into 3.5 nm Au colloid (prepared according to the method reported by Jana et al. [35]) for the required time or into 70 nm Au colloid (prepared according to the method reported by Frens [36]) for 24 h (Step III). Then, the substrates were immersed in a gold electroless deposition solution [37] (0.1 wt% $HAuCl_4$ and 0.4 mM hydroxylamine hydrochloride) for required time (Step IV). The PS template was removed using tetrahydrofuran (Step V).

3. Results and discussion

Fig. 1 showed the UV–vis spectra of Au sol and Au nanoparticles films at different assembly time. The PS array template was dissolved with tetrahydrofuran. It can be seen that the extinction peak of Au nanoparticle films dramatically shifted and broadened compared with Au nanoparticles in water. It is well known that the extinction of noble metal nanoparticles is closely related to the interparticle coupling [38]. The shift and broadening of the peaks shown in Fig. 1 therefore revealed intensive aggregation and strong interaction between adsorbed Au nanoparticles. As shown, the change in extinction peaks of Au nanoparticle films became slow as the adsorption time was prolonged, indicating that the amount of adsorbed Au nanoparticles tended to saturation. The absorbance of the UV–vis spectrum of nonporous Au nanoparticle films prepared without using the PS template was higher than that of porous Au nanoparitcle films of the same geometric size, indicating that the amount of Au nanoparticles in nonporous films was more than that in porous films. We can preliminarily conclude from the UV–vis spectra that the PS template well plays its role in adsorbing Au nanoparticles only in the interstice. The unique optical property of Au nanoparticles made the formation of Au nanoparitcle films easy to be monitored and controlled.

Fig. 2a showed a tilted SEM photograph of a 2D array of 530-nm PS particles on a $(PDDA/PSS)_2PDDA$ modified substrate. The SEM image showed that PS particles had a closely hexagonal packing fashion, demonstrating the efficiency of the self-assembly process at the interface in preparation of a 2D PS array. The PDDA functionalized surface has demonstrated high efficiency in immobilizing negatively charged colloidal particles [39]. Fig. 2b showed the top-view SEM image of the $(PDDA/PSS)_2PDDA$-modified slide after it was immersed in 3.5-nm colloidal Au suspension for 6 h and subsequently the PS array was removed from it using tetrahydrofuran. The image revealed that 3.5 nm-Au nanoparticles had indeed formed a compact film structure with holes discretely distributed. In the presence of the PS template, Au nanoparticles must pass through the array template before reaching the supporting substrate surface and being immobilized on the PDDA surface. The available entrance to the 2D PS array was the interstice between three PS particles. This type of entrance had a distance of a single-sphere diameter for transferring Au nanoparticles and could be very effective for Au suspension transport. Fig. 2c showed the SEM image of 70 nm Au nanoparticle film and the inset showed a magnified SEM image. Obviously, the Au nanoparticle size could affect the film appearance to a large extent. The thickness of the

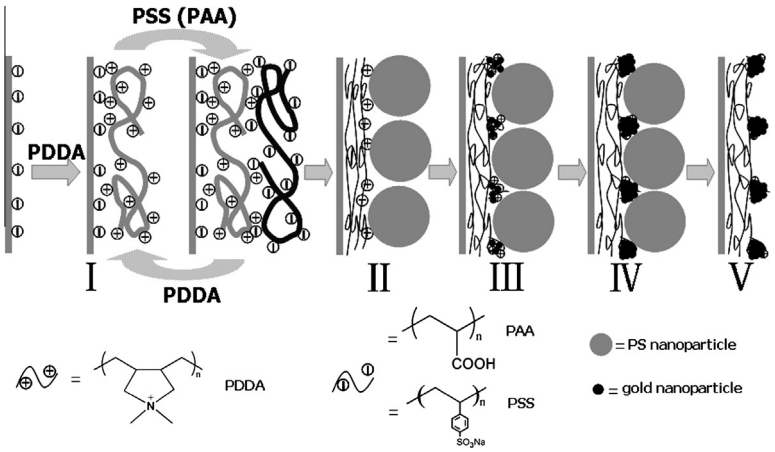

Scheme 1. Fabrication process of 2D conductive porous Au films.

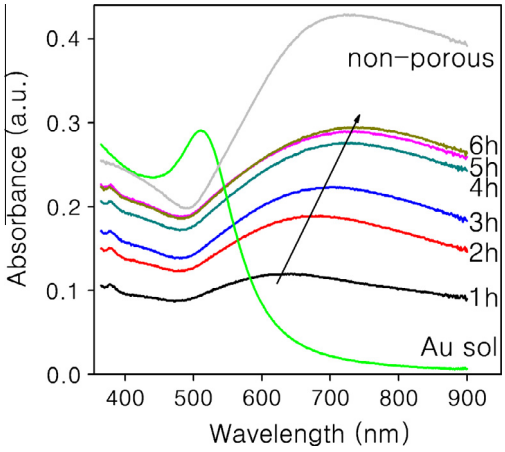

Fig. 1. UV–vis spectra of 3.5 nm Au nanoparticles in water (Au sol) and on a $(PDDA/PSS)_2PDDA$ modified surface with the PS array template (1–6 h) and without the PS array template (non-porous). The PS array template had been removed using tetrahydrofuran prior to spectroscopic characterization.

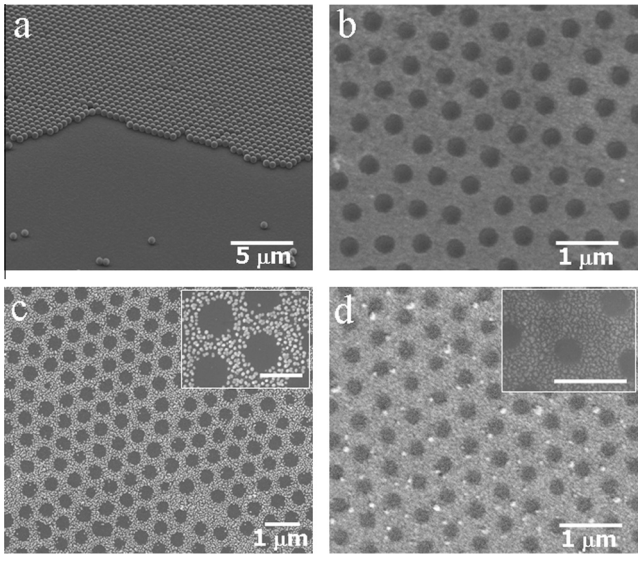

Fig. 2. SEM image of (a) tilted-view SEM of 530-nm PS array, (b) 3.5 nm Au particle film and (c) 70 nm Au particle on the $(PDDA/PSS)_2PDDA$ surface, and (d) 3.5 nm Au particle on the PDDA surface after the PS array was removed. The scale bars in the insets of (c) and (d) are both 600 nm.

PDDA layer serving as a fully charged PE in the PE multilayer film is no more than 10 nm, as reported by Decher [40]. The 10-nm thick PDDA layer may be sufficient to neutralize the surface charge of 3.5 nm Au nanoparticles, giving rise to densely adsorbed Au nanoparticles. In contrast, as the size of the Au nanoparticle increased to 70 nm, the PDDA chains were unable to completely offset the repulsive force between large Au nanoparticles, resulting in discretely distributed Au nanoparticles. Fig. 2d showed 3.5-nm Au nanoparticle film formed on PDDA layer modified substrate. The surface of the formed Au nanoparticle film was rougher than one in Fig. 2b. The close-up image showed in the inset of Fig. 2d revealed that Au nanoparticles formed discrete island-like aggregates. It was obvious that the structural diversity of PE layers was crucial to the morphological difference between Au nanoparticle films. It has been reported that the adsorption of a fully charged PE on an oppositely charged surface is affected by the surface charge density of a substrate [41]. For the $(PDDA/PSS)_2PDDA$ substrate, the PSS layer worked in an adsorption mode with abundant loops, which endowed the surface with a high density of negative charge compared with the bare glass slide. The folding configuration of PSS could adsorb PDDA of a relatively thick layer, and therefore loopy and folded chains of the PDDA layer could neutralize the repulsion force between Au nanoparticles to a large extent, resulting in a dense and smooth Au nanoparticle film. In contrast, the very smooth surface of the bare glass slide could only adsorb a very thin PDDA layer, resulting in discrete adsorption of Au nanoparticles. From the SEM characterization results, it was reasonable to conclude that the 2D array of PS particles was effective to induce Au nanoparticles to form reverse structures with respect to the template.

Fig. 3 showed the UV–vis spectra of 530 nm PS template/porous Au films with different Au electroless growth time. As the growth time was prolonged, the spectra of the ordered array changed drastically. The most significant feature after electroless growth of Au was the appearance of the peaks located at about 830 nm. This band was a unique feature of structured Au films, as shown in Fig. S1. Other peaks, such as peaks I and II, gradually shifted with increased Au growth duration. Peak positions of bands III and IV did not change after emergence. The rises of new peaks and shifts of peak positions indicated that reductive deposition of Au altered the refractive index of the PS array/Au nanoparticle films and resulted in dispersion change of the surface modes of complex array [42]. In contrast, the UV–vis spectra of non-porous Au film obtained after 10 min Au growth was featureless. This result indicated that based on the unique optical response of the ordered PS array template, UV–vis spectroscopy was a very simple and effec-

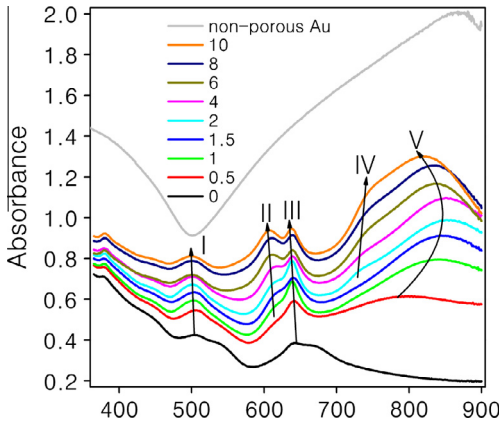

Fig. 3. UV–vis spectra of the non-porous Au film with 10 min Au electroless deposition and the PS template/Au nanoparticle complex array after different Au electroless deposition time. The deposition time (in min) was labeled by the corresponding Arabic numbers.

tive method to monitor the electroless deposition of Au under the catalysis of Au nanoparticles.

The SEM image of 530 nm PS template/Au nanoparticles array after a 10-min Au electroless deposition (Fig. 4a) revealed that there was no Au on the PS surface. Fig. 4a also indicated that Au nanoparticles had an excellent catalytic ability to guide selective deposition of Au from the solution to its surface. Fig. 4b and c showed the porous gold films made on PDDA and $(PDDA/PSS)_2$-PDDA modified substrates using 530 nm PS template, respectively. Fig. 4d showed the SEM image of the porous Au film obtained from 70 nm Au nanoparticle film on the $(PDDA/PSS)_2PDDA$ surface. It was obvious that the surface shown in Fig. 4c was smoother than that shown in Fig. 4b and d. Compared with Fig. 3, a logical relationship can be found between surface morphologies of conductive porous Au films and Au nanoparticle films, i.e. the discrete and compact Au nanoparticle films corresponded to rough and smooth conductive porous Au films, respectively. The difference in surface roughness of ultimate conductive Au films could be interpreted by

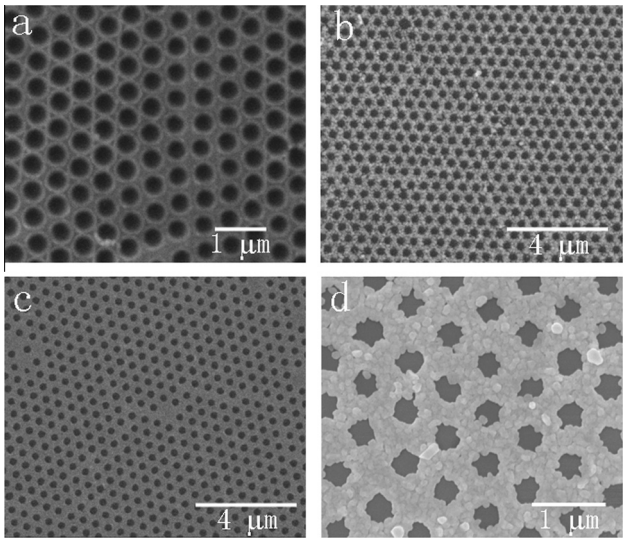

Fig. 4. SEM image of (a) 530 nm PS array/3.5 nm Au nanoparticles after 10 min Au electroless deposition, (b) conductive porous Au film formed from 3.5 nm Au nanoparticle film on the PDDA surface, (c) conductive porous Au film formed from 3.5 nm Au nanoparticle film on the $(PDDA/PSS)_2PDDA$ surface using 530 nm PS array, and (d) conductive porous Au film from 70 nm Au nanoparticle film on the $(PDDA/PSS)_2PDDA$ surface using 750 nm PS array template.

Au nanoparticle catalyzed deposition. Discrete Au nanoparticle aggregates and large Au nanoparticles needed to continuously grow to touch each other to produce a rough surface, and as a consequence, the roughness increased with the enlargement of a discrete building block. The densely adsorbed Au nanoparticles, in contrast, made themselves easy to merge into a whole without requiring distinct enlargement of Au nanoparticles, leading to a relatively smooth surface. The use of an ordered 2D PS template could not only obtain conductive Au films with an ordered hole array, but also facilitate formation of a smooth surface (Fig. S2).

The present method for the fabrication of porous Au films mainly included four steps, and in each step, the structures of porous Au films, including film thickness, hole diameter, and ratio of hole diameter to wall thickness (D/W) could be adjusted by regulating parameters. Most straightforwardly, the thickness of porous films could be adjusted by controlling the electroless growth time (Fig. S3). In addition, the film thickness of conductive porous Au could also be regulated by controlling self-assembly of PEs. Fig. 5a and b showed the AFM images of conductive porous Au films fabricated from 3.5-nm Au nanoparticle films on the $(PDDA/PSS)_2PDDA$ and $(PDDA/PAA)_2PDDA$ modified substrates, respectively. Based on line scan analysis, we could find that the film thickness in Fig. 5a and b was 31 nm and 55 nm, respectively. The only different parameter in the fabrication process for the two types of Au films was the intermediate component of the three-layer structured PE functional layers. The three PE functional layers in Fig. 5a was comprised fully ionized polyelectrolyte PDDA and PSS. Both types of polyelectrolyte layers were assembled from the solution containing 1 mg/mL PE and 0.5 M NaCl. It has been

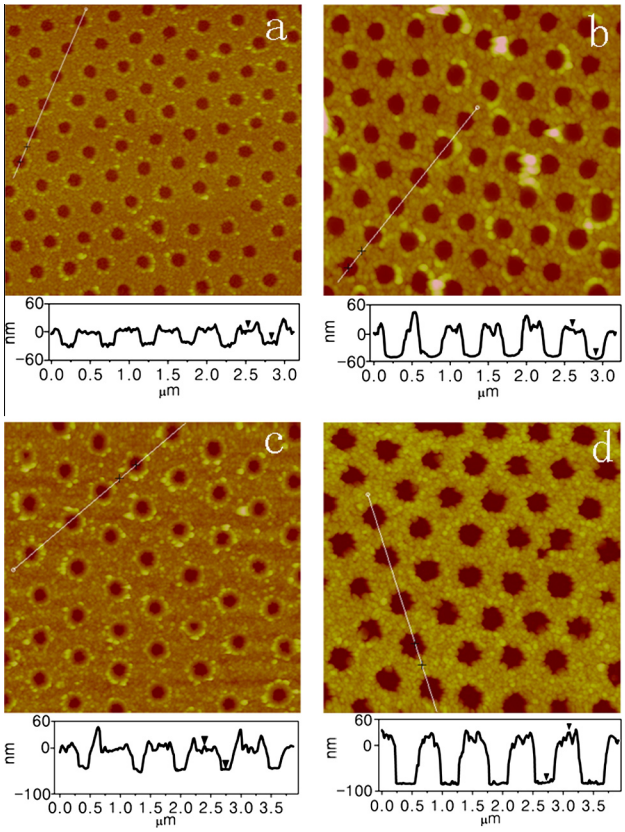

Fig. 5. AFM images of conductive porous Au films fabricated (a) on the $(PDDA/PSS)_2PDDA$ and (b) on the $(PDDA/PAA)_2PDDA$ surface modified with 530-nm PS/3.5 nm Au nanoparticle array, (c) from 3.5 nm and (d) from 70 nm Au nanoparticle on the $(PDDA/PAA)_2PDDA$ surface using 750-nm PS template. All line scan analyses were obtained along white lines.

reported that the thickness of one layer-pair of two fully charged PE components is no more than 17 nm with 1 M electrolyte concentration [40] and one could therefore deduce that the thickness of the PDDA surface layer should not exceed 10 nm. The thin PDDA layer could only adsorb a thin layer of Au nanoparticles, leading to the result as shown in Fig. 5a. The middle PE layer in Fig. 5b was PAA, a weak polyelectrolyte, and its adsorption thickness could reach 30 nm with many loops and tails at pH 2.5, as reported by Yoo et al. [41]. In the overcompensation process of surface charge, the PDDA molecules wrapped PAA chains and formed a thick layer. The 3.5-nm Au nanoparticles could be adsorbed by loopy PDDA chains, resulting in increased thickness of Au nanoparticles films, so that a thicker conductive porous Au film could be generated after the electroless deposition process.

The thickness of a porous Au film could also be adjusted by changing the Au nanoparticle size in the formation process of Au nanoparticle films. Fig. 5c and d showed the AFM images of conductive porous Au films fabricated from 3.5 nm and 70 nm Au nanoparticle films on 750 nm PS array/$(PDDA/PAA)_2$PDDA surface, respectively. As can be seen, the thickness of the two types of porous Au films was 55 nm and 110 nm, respectively. The contrast in Fig. 5c and d indicated that controlling the size of Au nanoparticles was an effective path to change structural parameters of porous Au films. By comparing Fig. 5a–b and comparing c–d, one can find that the lattice structure of nanohole arrays could remain constant when the film thickness was changed. With 2D arrays of PS spheres with different diameters used as templates and PE films with of the same structure as the coupling layer (Fig. 5b and c), the dispersion of the nanohole lattice structure could be adjusted when the film thickness was kept constant.

The hole diameter on a conductive porous Au film could be facilely adjusted using PS templates with different sizes (Fig. S4). Furthermore, one could find from AFM analysis that the hole diameters changed with the variation of porous Au film thickness. For examples, the hole diameter increased from 242 nm to 290 nm when film thickness increased from 31 nm to 55 nm, as shown in Fig. 5a and b. Fig. 5c and d also illustrated a drastic increase in the hole diameter with the augmentation of film thickness (hold diameters of 385 nm and 450 nm corresponding to film thickness of 53 nm and 110, respectively). Especially, Fig. 5d showed that nanoholes on the porous Au film had a steep side wall. This feature was quite different from porous metallic films prepared by electrochemical deposition and the traditional electroless deposition method in which metal is deposited tightly around the template spheres and forms a concave inner surface [18]. It was deduced that the phenomenon was caused by large Au nanoparticles around PS particles, which could not enter the narrow gap between the PS spheres and the supporting substrate. Therefore, there was no Au deposited in the narrow gap in the electroless deposition step, resulting in nearly the same size of the hole diameters on the back and front surfaces, which was the feature of a hole with a steep side wall. The strategy of pre-assembly of Au nanoparticles into a porous film followed by electroless deposition to fabricate a porous Au film is distinctive in controlling the hole structure because the influence of the spherical shape of the polystyrene particle template was suppressed compared with electrodeposition and the traditional electroless deposition method. Compared with combination of etching with physical deposition for preparing porous metal films, the method of Au nanoparticle catalyzed Au deposition was quite easy to operate in adjusting the structures of porous Au films because the surface roughness, film thickness, and hole diameters can be flexibly regulated just by controlling the assembly of polyelectrolyte and Au nanoparticles without any requirement for additional pretreatment operations.

Using heating treatment, the nanohole diameter could be independently adjusted without changing the film thickness and lattice structure. Under this condition, the change of the hole diameter was always accompanied by the variation of the hole wall. Therefore, the ratio of the hole diameter to the wall thickness (D/W) was utilized to describe the effect of heating treatment. As shown in Fig. 5a, the D/W value for porous Au films fabricated on the $(PDDA/PSS)_2$PDDA substrate without heating treatment was 0.83. The minimum D/W value for porous Au films obtained on the $(PDDA/PAA)_2$PDDA substrate (Fig. 5b) was greater than 0.83 because the increase in the film thickness resulted in an enlargement of the hole diameter and decrease of the wall thickness. The D/W value for conductive porous Au films gradually increased when the heating treatment to the PS template was prolonged. Fig. 6a showed the TEM image of conductive porous Au film obtained by using a PS template heated on a 120 °C hotplate for 7 min, which resulted in a D/W value of 2.3. A heating duration longer than 7 min at 120 °C could cause blocking of the top entrance and loss of template functions. A higher treatment temperature could easily lead to a fast melting phenomenon of PS particles, which made this step difficult to control. Fig. 6b showed the curve of D/W versus heating time, the slope of which represented the change rate of D/W. It was found that the curve became increasingly steeper when the duration is longer than 3 min. The variation trend of D/W shown in Fig. 6b was closely related to the heating fashion of the hotplate. The hotplate heating treatment was quite different from the operation in an oven in which the whole PS particles were heated by high temperature atmosphere [43]. As a contrast, the PS particle on a hotplate started to melt from its bottom only when the temperature of the support

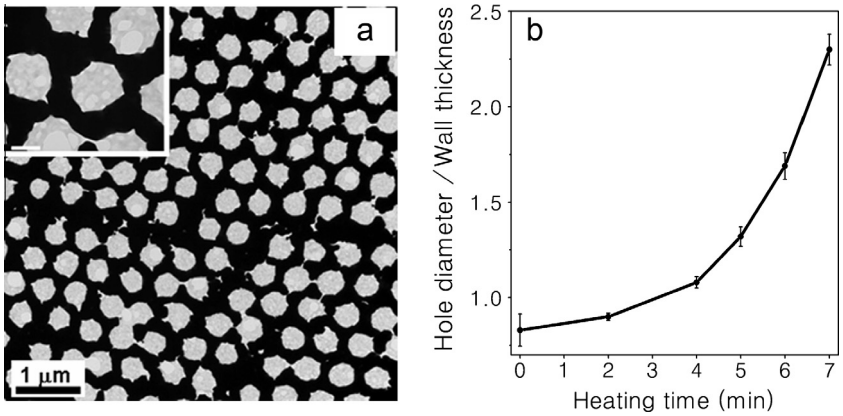

Fig. 6. (a) TEM image of conductive porous Au films obtained by heating the 530-nm PS array/$(PDDA/PSS)_2$PDDA substrate on a hotplate at 120 °C for 7 min. The scale bar in the inset is 200 nm. (b) Plot of the hole diameter/wall thickness ratio (D/W) versus heating time.

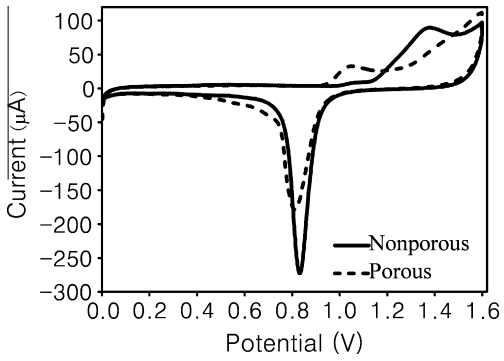

Fig. 7. Cyclic voltammograms of 55-nm thick conductive porous Au film (dashed line) and non-porous conductive Au film (solid line). The electrolyte was a 0.1 M H_2SO_4 solution and the scan rate was 100 mV/S.

substrate reached its glass transition temperature (Tg). This process needed a certain time length to heat the support substrate from room temperature to Tg, which was reflected at the beginning of the curve in Fig. 6b. Once the substrate temperature exceeded Tg of PS, the gradually increasing temperature leaded the melting rate of the PS particles to accelerate, as shown in the latter half of Fig. 6b.

The 55-nm porous Au film fabricated using 530 nm-PS template and the nonporous Au film prepared with the same method was scanned in a 0.1 M H_2SO_4 solution with a scan rate of 100 mV s^{-1}. Fig. 7 showed the cyclic voltammograms. In the positive sweep, the onset of gold oxidation began from 0.95 V (versus SCE). The oxidized gold was electrochemically reduced in the negative sweep with a peak potential of 0.83 V. The ratio of integrated charge between the porous Au and nonporous Au films of the same geometrical size was 0.88, which should equal to the ration of their effective surfaces if all the surfaces of the porous Au films participated in the electrochemical reaction [44]. From the AFM result (Fig. 5b), it could be calculated that the ratio of the exposed surface of the conductive porous Au film (sum of the geometrical sizes of the Au mesh and its side wall area) to the surface area of the nonporous Au film was 0.92. The approximate consistency between the two values indicated that all the surface areas of the porous Au film were accessible for the electrolyte solution, i.e. all the surfaces of the porous Au mesh could support electrochemical reactions.

4. Conclusions

The structure consisting of 2D arrays of PS particles immobilized on the PE layer modified substrate was proven very effective to induce Au nanoparticles to form 2D ordered porous film which acted as the catalyst for electroless growth of gold. The structural confinement effect of the primary PS array template and the catalysis constraint effect of the secondary porous Au nanoparticle template made the porous Au preparation strategy very compact and effective. Using Au nanoparticles as the building block and PE layer as the coupling reagent, we revealed that a slight change in Au nanoparticles and PE structures could lead to an obvious change in the structures of both the porous Au nanoparticle films and conductive porous Au films. Electrochemical CV on conductive porous Au films indicated all surfaces of the 2D array were accessible in a solution.

Acknowledgment

We gratefully acknowledge the financial support from National Natural Science Foundation of China (21175051, 21375043).

Appendix A. Supplementary material

Supplementary data associated with this article can be found, in the online version, at http://dx.doi.org/10.1016/j.jcis.2014.09.058.

References

[1] T.W. Ebbesen, H.J. Lezec, H.F. Ghaemi, T. Thio, P.A. Wolff, Nature 391 (1998) 667.
[2] J.C. Sharpe, J.S. Mitchell, L. Lin, N. Sedoglavich, R.J. Blaikie, Anal. Chem. 80 (2008) 2244.
[3] A.A. Yanik, M. Huang, O. Kamohara, A. Artar, T.W. Geisbert, J.H. Connor, H. Altug, Nano Lett. 10 (2010) 4962.
[4] A.G. Brolo, E. Arctander, R. Gordon, B. Leathem, K.L. Kavanagh, Nano Lett. 4 (2004) 2015.
[5] A.G. Brolo, S.C. Kwok, M.G. Moffitt, R. Gordon, J. Riordon, K.L. Kavanagh, J. Am. Chem. Soc. 127 (2005) 14936.
[6] J.H. Li, S.W. Chen, Y. Chou, M.C. Wu, C.H. Hsueh, W.F. Su, J. Phys. Chem. C 115 (2011) 24045.
[7] R.M. Cole, J.J. Baumberg, F.J. Garcia de Abajo, S. Mahajan, M. Abdelsalam, P.N. Bartlett, Nano Lett. 7 (2007) 2094.
[8] G. Hong, C. Li, Q. Limin, Adv. Funct. Mater. 20 (2010) 3774.
[9] H. Lee, J. Park, J. Kim, H. Jung, T. Kawai, Appl. Phys. Lett. 89 (2006) 113901.
[10] T. Lohmuller, U. Muller, S. Breisch, W. Nisch, R. Rudorf, W. Schuhmann, S. Neugebauer, M. Kaczor, S. Linke, S. Lechner, J. Spatz, M. Stelzle, J. Micromech. Microeng. 18 (2008) 115011.
[11] J. van de Groep, P. Spinelli, A. Polman, Nano Lett. 12 (2012) 3138.
[12] H.Y. Jang, S.K. Lee, S.H. Cho, J.H. Ahn, S. Park, Chem. Mater. 25 (2013) 3535.
[13] T. Gao, B. Wang, B. Ding, Nano Lett. 14 (2014) 2105.
[14] Z. Huang, H. Fang, J. Zhu, Adv. Mater. 19 (2007) 744.
[15] L. Wu, W. He, D. Teng, S. Ji, C. Ye, Langmuir 28 (2012) 7476.
[16] J. Rundqvist, J.H. Hoh, D.B. Haviland, Langmuir 22 (2006) 5100.
[17] S.H. Lee, K.C. Bantz, N.C. Lindquist, S.H. Oh, C.L. Haynes, Langmuir 25 (2009) 13685.
[18] F. Sun, W.P. Cai, Y. Li, B. Cao, F. Lu, G. Duan, L. Zhang, Adv. Mater. 16 (2004) 1116.
[19] T. Yonezawa, S. Onoue, N. Kimizuka, Adv. Mater. 13 (2001) 140.
[20] P.S. Shah, M.B. Sigman, C.A. Stowell, K.T. Lim, K.P. Johnston, B.A. Korgel, Adv. Mater. 15 (2003) 971.
[21] A.E. Saunders, P.S. Shah, M.B. Sigman, T. Hanrath, H.S. Hwang, K.T. Lim, K.P. Johnston, B.A. Korgel, Nano Lett. 4 (2004) 1943.
[22] J. Li, J. Peng, W. Huang, Y. Wu, J. Fu, Y. Cong, L. Xue, Y. Han, Langmuir 21 (2005) 2017.
[23] L. Kong, R. Dong, H. Ma, J. Hao, Langmuir 29 (2013) 4235.
[24] H.L. Cong, W.X. Cao, Adv. Funct. Mater. 15 (2005) 1821.
[25] Y. Li, G. Duan, G. Liu, W. Cai, Chem. Soc. Rev. 42 (2013) 3614.
[26] K. Leong, Y. Chen, D.J. Masiello, M.T. Zin, M. Hnilova, H. Ma, C. Tamerler, M. Sarikaya, D.S. Ginger, A.K.Y. Jen, Adv. Funct. Mater. 20 (2010) 2675.
[27] C.L. Haynes, R.P. Van Duyne, J. Phys. Chem. B 105 (2001) 5599.
[28] C.M. Hsu, S.T. Connor, M.X. Tang, Y. Cui, Appl. Phys. Lett. 93 (2008) 133109.
[29] Y. Li, J. Zhang, S. Zhu, H. Dong, F. Jia, Z. Wang, Y. Tang, L. Zhang, S. Zhang, B. Yang, Langmuir 26 (2010) 9842.
[30] B. Wang, H. Gao, J. Lau, S. Chua, Appl. Phys. A 107 (2012) 139.
[31] F. Sun, W. Cai, Y. Li, B. Cao, Y. Lei, L. Zhang, Adv. Funct. Mater. 14 (2004) 283.
[32] B.J.Y. Tan, C.H. Sow, T.S. Koh, K.C. Chin, A.T.S. Wee, C.K. Ong, J. Phys. Chem. B 109 (2005) 11100.
[33] A. Kosiorek, W. Kandulski, H. Glaczynska, M. Giersig, Small 1 (2005) 365.
[34] Z.C. Lu, M. Zhou, J. Colloid Interface Sci. 361 (2011) 429.
[35] N.R. Jana, L. Gearheart, C.J. Murphy, Langmuir 17 (2001) 6782.
[36] G. Frens, Nature 241 (1973) 20.
[37] H. Menzel, M.D. Mowery, M. Cai, C.E. Evans, Adv. Mater. 11 (1999) 131.
[38] K.C. Grabar, R.G. Freeman, M.B. Hommer, M.J. Natan, Anal. Chem. 67 (1995) 735.
[39] X. Li, W. Xu, J. Zhang, H. Jia, B. Yang, B. Zhao, B. Li, Y. Ozaki, Langmuir 20 (2004) 1298.
[40] G. Decher, J. Schmitt, Prog. Colloid Polym. Sci. 89 (1992) 160.
[41] D. Yoo, S.S. Shiratori, M.F. Rubner, Macromolecules 31 (1998) 4309.
[42] H.T. Miyazaki, H. Miyazaki, K. Ohtaka, T. Sato, J. Appl. Phys. 87 (2000) 7152.
[43] Y. Li, W. Cai, B. Cao, G. Duan, C. Li, F. Sun, H. Zeng, J. Mater. Chem. 16 (2006) 609.
[44] X. Chen, Y. Wang, J. Zhou, W. Yan, X. Li, J.J. Zhu, Anal. Chem. 80 (2008) 2133.